



POTSDAM-INSTITUT FÜR
KLIMAFOLGENFORSCHUNG

Originally published as:

Schultz, D., Spiegel, S., Marwan, N., Albayrak, S. (2015): Approximation of diagonal line based measures in recurrence quantification analysis. - Physics Letters A, 379, 14-15, 997-1011

DOI: [10.1016/j.physleta.2015.01.033](https://doi.org/10.1016/j.physleta.2015.01.033)

Available at <http://www.sciencedirect.com>

© Elsevier

Approximation of diagonal line based measures in recurrence quantification analysis

D. Schultz^{a,*}, S. Spiegel^a, N. Marwan^b, S. Albayrak^a

^a*DAI-Lab, Berlin Institute of Technology, Ernst-Reuter-Platz 7, 10587 Berlin, Germany*

^b*Potsdam Institute for Climate Impact Research, 14412 Potsdam, Germany*

Abstract

Given a trajectory of length N , recurrence quantification analysis (RQA) traditionally operates on the recurrence plot, whose calculation requires quadratic time and space ($\mathcal{O}(N^2)$), leading to expensive computations and high memory usage for large N . However, if the similarity threshold ε is zero, we show that the recurrence rate (RR) and many diagonal line based RQA-measures, e.g., the determinism (DET), can be obtained algorithmically taking $\mathcal{O}(N \log(N))$ time and $\mathcal{O}(N)$ space. Furthermore, for the case of $\varepsilon > 0$ we propose approximations to the RQA-measures that are computable with same complexity. Experiments with autoregressive systems show that the approximation error is small if the dimension of the trajectory and the minimum diagonal line length are small. When applying the approximate determinism to the problem of detecting dynamical transitions we observe that it performs as well as the exact determinism measure.

Keywords: Recurrence quantification analysis, Recurrence plot, Determinism, Approximation, Phase space discretization

1. Introduction

2 Recurrence quantification analysis (RQA), i.e., the quantification of struc-
3 tures in recurrence plots [1], has established in several fields of research as a
4 powerful tool to investigate recurrence related properties of complex dynamical
5 systems [2]. The popularity of RQA is founded in its simplicity and flexibility
6 to be applied to almost any type of data, including non-stationary processes
7 [3]. In particular the outstanding role of the RQA-measure *determinism* (DET)
8 has been demonstrated in several applications, including discriminating signals
9 from noise [4], detecting dynamical transitions [5, 6], and the recently proposed
10 use for pattern mining and classification [7]. A comprehensive overview of re-
11 currence plots and its applications is given in [1].

*Corresponding author

Email address: schultz@dai-lab.de (D. Schultz)

12 The computation and quantification of recurrence plots generally involves
13 operations with quadratic time and space complexity ($\mathcal{O}(N^2)$). This computa-
14 tional complexity leads to strongly increasing computation times and memory
15 consumption for long time series (longer than 100,000 data points). Recurrence
16 analysis of long time series, such as audio data [8], epileptic seizures [9], material
17 damage detection [10], or hourly weather variability [11], is, therefore, limited.
18 Another application that can be limited by the high computational complexity
19 is online monitoring of data streams, e.g., for video surveillance [12], monitoring
20 social interactions [13], or assessing driving behavior [7]. Parallel computing
21 approaches (e.g., using GPU calculations [11, 14]) can accelerate computation
22 but do not reduce the computational complexity.

23 In this letter we show the following. If the similarity threshold ε is zero,
24 then the recurrence rate and many diagonal line based RQA-measures, e.g., the
25 determinism, are in the computational complexity class $\mathcal{O}(N \log(N))$, whereas
26 space complexity is $\mathcal{O}(N)$. We use this observation in order to propose approxi-
27 mations to these measures for the case of $\varepsilon > 0$. The (approximative) measures
28 are obtained algorithmically, without having to calculate the recurrence plot.

29 2. Motivation

30 Recent work has introduced recurrence plot-based distance measures, which
31 can be utilized for mining (multi-dimensional) time series with nonlinear dynam-
32 ics [15, 16]. However, the quadratic time and space complexity of computation
33 and quantification of recurrence plots makes distance calculations for relatively
34 long time series and online processing of fast time series streams intractable.
35 For these purposes we aim to approximate the proposed recurrence plot-based
36 distance measures in such a way as to reduce the computational complexity
37 while maintaining the classification accuracy.

38 3. Recurrence quantification analysis

39 For a given d -dimensional phase space trajectory \vec{x} (reconstructed from a
40 time series x , e.g., by time-delay embedding [17]) of length N and similarity
41 threshold $\varepsilon \geq 0$ the recurrence plot of \vec{x} is an illustration of the binary recurrence
42 matrix \mathbf{R} , given by

$$43 \quad R_{i,j} = \Theta(\varepsilon - \|\vec{x}_i - \vec{x}_j\|), \quad i, j = 1, \dots, N,$$

44 where $\|\cdot\|$ is a norm in the phase space of \vec{x} and Θ is the Heaviside step function,
45 defined by $\Theta(y) = 1$ if $y \geq 0$ and $\Theta(y) = 0$ if $y < 0$. Thus Θ indicates whether
46 \vec{x}_i and \vec{x}_j are in ε -proximity (also denoted as similar) or not, i.e., $R_{i,j} = 1$
47 if $\|\vec{x}_i - \vec{x}_j\| \leq \varepsilon$ and $R_{i,j} = 0$ if $\|\vec{x}_i - \vec{x}_j\| > \varepsilon$. This relation is essential for
48 the study of recurrence plots and will be used extensively in this letter. The
49 recurrence plot contains the *line of identity (LOI)*, which means that each entry
50 on the main diagonal of \mathbf{R} is 1. Structures parallel to the main diagonal, referred

51 to as diagonal lines, are caused by similarly evolving epochs of the phase space
 52 trajectory \vec{x} .

53 Recurrence quantification analysis was developed in order to quantitatively
 54 describe recurrence plots. For this purpose, small scale structures, such as
 55 recurrence points or diagonal lines in the recurrence plot are used [18]. The
 56 fraction of recurrence points in the recurrence plot is measured by the *recurrence*
 57 *rate*,

$$58 \quad RR = \frac{1}{N^2} \sum_{i,j=1}^N R_{i,j}, \quad (1)$$

59 which is interpreted as the probability to find a recurrence of trajectory \vec{x} . A
 60 more sophisticated RQA-measure is the *determinism*, which is defined for a
 61 given minimum diagonal line length μ as

$$DET^{(\mu)} = \frac{\sum_{l=\mu}^N l \cdot P(l)}{\sum_{i,j=1}^N R_{i,j}}, \quad (2)$$

62 where $P(l)$ is the number of diagonal lines of length l in \mathbf{R} . DET can be
 63 interpreted as the probability that a recurrence point belongs to a diagonal
 64 line. The parameter μ is usually set to 2. This choice is sufficient for most
 65 applications. However, in particular cases, larger values of μ can be necessary,
 66 e.g., reducing effects of tangential motion (oversampling), noise, or embedding
 67 effects [1].

68 As already mentioned, a phase space trajectory of a univariate time series
 69 can be reconstructed by time delay embedding [17]. We call this procedure *time*
 70 *series embedding*, since it is applied to the time series. In the sequel we will
 71 apply the method of time delay embedding to the trajectory \vec{x} (that possibly
 72 was created by time series embedding for reconstruction purposes), but with
 73 the intention of quantifying diagonal structures in \mathbf{R} . In order to distinguish
 74 that from the time series embedding, we will denote this as *trajectory embedding*.
 75 More precisely, for a fixed time delay 1 and embedding dimension ν , we consider
 76 the trajectory embedding vectors

$$\vec{x}_j^\nu = (\vec{x}_j, \vec{x}_{j+1}, \dots, \vec{x}_{j+\nu-1}), \quad (3)$$

77 which are of dimension $d \cdot \nu$, provided that the trajectory \vec{x} is d -dimensional. The
 78 trajectory embedding of \vec{x} is then defined to be the sequence $\vec{x}^\nu = (\vec{x}_j^\nu)_{j=1, \dots, N-\nu+1}$,
 79 which can be imagined as a trajectory in a $(d \cdot \nu)$ -dimensional phase space. In
 80 Sec. 4.2 we show that information about $P(l)$ can be extracted by these repre-
 81 sentations leading to a surprising identity for the determinism.

82 4. RR and DET identities

83 We deduce identities for RR and $DET^{(\mu)}$, which allow fast calculation (with-
 84 out computing the recurrence plot) if the similarity threshold ε is zero. The
 85 identity for RR does hold for $\varepsilon = 0$ only. The identity for $DET^{(\mu)}$ is first shown

86 for arbitrary $\varepsilon \geq 0$ and the assumption that the phase space norm is the maxi-
 87 mum norm $\|\cdot\|_\infty$. However, in the special case of $\varepsilon = 0$, we will argue that the
 88 restriction to the $\|\cdot\|_\infty$ -norm becomes redundant. Consequently it follows the
 89 important fact that the recurrence rate and the determinism are in $\mathcal{O}(N \log(N))$
 90 if $\varepsilon = 0$, whereas the computational complexity of the classical methods that
 91 quantify the recurrence plot is $\mathcal{O}(N^2)$.

92 4.1. Recurrence rate identity

93 Given the trajectory embedding \vec{x}^ν , Eq. (3), in analogy to Eq. (1) we define

$$\mathcal{PP}^{(\nu)} := \sum_{i,j=1}^{N-\nu+1} \Theta(\varepsilon - \|\vec{x}_i^\nu - \vec{x}_j^\nu\|), \quad (4)$$

94 the number of pairwise proximities of the elements in \vec{x}^ν . Note that $RR =$
 95 $\mathcal{PP}^{(1)}/N^2$ is the recurrence rate of \vec{x} and more general $\mathcal{PP}^{(\nu)}/(N-\nu+1)^2$ is
 96 the recurrence rate of \vec{x}^ν .

97 If nominal recurrences [19] are in demand, that is $\varepsilon = 0$, then $\mathcal{PP}^{(\nu)}$ (and
 98 thus the recurrence rate RR) can be determined efficiently, i.e., with algorithmic
 99 complexity of $\mathcal{O}(N \log(N))$. In order to achieve this complexity, we employ the
 100 histogram h_X of the trajectory embedding vectors $X := \vec{x}^\nu$, which is given by

$$h_X : Y \rightarrow \mathbb{N}, \quad \vec{y} \mapsto \sum_{\vec{x} \in X} \Theta(-\|\vec{x} - \vec{y}\|),$$

101 where Y is the set of unique members of X .

102 **Theorem 1.** *Let $X = \vec{x}^\nu$ be the sequence of trajectory embedding vectors as*
 103 *defined in Eq. (3) and denote by h_X the histogram of the elements in X . If*
 104 *$\varepsilon = 0$, then*

$$\mathcal{PP}^{(\nu)} = \sum_{\vec{y} \in Y} (h_X(\vec{y}))^2. \quad (5)$$

105 **PROOF.** First note that a similarity (or proximity) corresponds to an equality
 106 if $\varepsilon = 0$, that is

$$\Theta(-\|\vec{x}_i^\nu - \vec{x}_j^\nu\|) = 1 \quad \Leftrightarrow \quad \vec{x}_i^\nu = \vec{x}_j^\nu.$$

107 The claim follows by simple combinatorial arguments. Assume that for $\vec{y} \in Y$
 108 there are exactly n elements in X that are equal to \vec{y} . Then there are n^2 pairwise
 109 equalities of these n elements, and hence n^2 pairwise proximities that increase
 110 $\mathcal{PP}^{(\nu)}$ by n^2 . But n is exactly determined by $h_X(\vec{y}) = n$. Taking the sum over
 111 all $\vec{y} \in Y$ yields the claim. \square

112 Based on this observation we can calculate the right hand side of Eq. (5)
 113 efficiently. The algorithmic details are discussed in Sec. 5.2.2.

114 *4.2. Determinism identity*

115 For the rest of this letter we choose the phase space norm $\|\cdot\|_\infty$, in particular
 116 we assume that \mathbf{R} and all $\mathcal{PP}^{(\nu)}$ are obtained for $\|\cdot\| = \|\cdot\|_\infty$. Then there is a
 117 relation between diagonal lines in the recurrence plot and recurrence points of
 118 trajectory embeddings. Before we formulate the determinism identity, we will
 119 give an intuition for the just mentioned relation: For a trajectory \vec{x} let \mathbf{R} be
 120 the recurrence plot. Consider the trajectory embedding \vec{x}^2 of \vec{x} of dimension
 121 $\nu = 2$ and the corresponding recurrence plot $\mathbf{R}^{(2)}$. Now, in the maximum norm,
 122 we have that $R_{i,j}^{(2)} = 1$ is equivalent to $R_{i,j} = R_{i+1,j+1} = 1$. In other words, a
 123 diagonal line of length 2 in \mathbf{R} corresponds to a recurrence point in $\mathbf{R}^{(2)}$, which
 124 is quantified by $\mathcal{PP}^{(2)}$.

125 **Theorem 2.** *Let μ be a choice of the minimum diagonal line length. For a*
 126 *trajectory \vec{x} , let the recurrence plot \mathbf{R} and the pairwise proximity measures*
 127 *$\mathcal{PP}^{(1)}, \mathcal{PP}^{(\mu)}, \mathcal{PP}^{(\mu+1)}$ be obtained for $\|\cdot\| = \|\cdot\|_\infty$. Then for arbitrary $\varepsilon \geq 0$*
 128 *it holds*

$$DET^{(\mu)} = \frac{\mu \cdot \mathcal{PP}^{(\mu)} - (\mu - 1) \cdot \mathcal{PP}^{(\mu+1)}}{\mathcal{PP}^{(1)}}. \quad (6)$$

129 **PROOF.** See Appendix A, Sec. 10.

130 In some cases the *LOI* of the recurrence plot should not be included in the
 131 histogram $P(l)$, i.e., $P(N)$ is set to zero. Then Theorem 2 holds true with a
 132 slight modification:

$$DET^{(\mu)} = \frac{\mu \cdot \mathcal{PP}^{(\mu)} - (\mu - 1) \cdot \mathcal{PP}^{(\mu+1)} - N}{\mathcal{PP}^{(1)}}.$$

133 For further considerations we assume that the *LOI* is included.

134 It is important to discuss the condition on the underlying phase space norm
 135 that compares the elements in \vec{x} . First of all, the statement from Theorem 2
 136 only holds for the $\|\cdot\|_\infty$ -norm. Depending on the application, a specific norm
 137 may be selected. Usually, the Euclidean norm $\|\cdot\|_2$ is considered, but also the
 138 maximum norm $\|\cdot\|_\infty$ is often used because it is computationally faster and
 139 allows to study recurrence plots analytically [1]. If $\varepsilon = 0$, then the statement
 140 holds for all norms since each norm $\|\cdot\|$ only indicates if \vec{x}_i and \vec{x}_j are equal,
 141 i.e., by definition of a norm we have that $\Theta(-\|\vec{x}_i - \vec{x}_j\|) = 1$ is equivalent to
 142 $\vec{x}_i = \vec{x}_j$.

143 Two observations from the proof of Theorem 2 describing the relation be-
 144 tween $P(l)$ and $\mathcal{PP}^{(\mu)}$ are worth mentioning here. Firstly,

$$\sum_{l \geq \mu} P(l) = \mathcal{PP}^{(\mu)} - \mathcal{PP}^{(\mu+1)}, \quad (7)$$

145 which is the number of diagonal lines in \mathbf{R} of minimal length μ , and secondly

$$\mathcal{PP}^{(\nu)} = \sum_{l \geq \nu} (l - \nu + 1) P(l).$$

146 By now, the identity in Theorem 2 does not provide a method to compute
 147 the determinism efficiently for general ε . However, if $\varepsilon = 0$, then $\mathcal{PP}^{(1)}$, $\mathcal{PP}^{(\mu)}$
 148 and $\mathcal{PP}^{(\mu+1)}$ can be calculated fast, as argued in Sec. 4.1, and then $DET^{(\mu)}$ is
 149 a simple algebraic computation in terms of these quantities.

150 It is worth to mention that the relationship between the length of diagonal
 151 lines in the recurrence plot and the embedding dimension is of more fundamen-
 152 tal nature. For example, the K_2 entropy can be directly estimated from the
 153 recurrence plot using the diagonal line lengths [1] instead of the dimension of
 154 the embedding dimension [20].

155 5. Approximation of RQA

156 Approximations for RR and $DET^{(\mu)}$ are presented that are computable in
 157 $\mathcal{O}(N \log(N))$. These approximative measures are obtained algorithmically, that
 158 means we do not calculate the recurrence plot. In Sec. 4, we have discussed
 159 the simplified case of $\varepsilon = 0$, where these measures are in the just mentioned
 160 complexity class. In this section we study the case of $\varepsilon > 0$, for which we
 161 propose a phase space discretization approach in order to approximate $\mathcal{PP}^{(\nu)}$.
 162 The discretization will generate the situation of a zero threshold, which allows
 163 us to apply the results from Sec. 4.

164 5.1. Approximation method

165 We propose to discretize the phase space for a grid size parameter $\delta > 0$ via

$$\Phi_\delta : \mathbb{R}^n \rightarrow \mathbb{Z}^n, \quad \vec{y} \mapsto \tilde{\vec{y}} := \left\lfloor \frac{\vec{y}}{\delta} \right\rfloor, \quad (8)$$

166 where n is an arbitrary natural number and $\lfloor \cdot \rfloor$ is the component-wise round off
 167 operation. Applying Φ_δ to the trajectory \vec{x} leads to a partition of the phase space
 168 in hypercubes of size δ . Then we replace the similarity condition $\|\vec{x}_i^\nu - \vec{x}_j^\nu\|_\infty \leq \varepsilon$
 169 by affiliation to the same cube, i.e., by the condition $\tilde{\vec{x}}_i^\nu = \tilde{\vec{x}}_j^\nu$. For convenience,
 170 we formulate this as a classification problem following the rules,

171 \vec{x}_i^ν and \vec{x}_j^ν are classified as . . .

- 172 (1) similar if $\Theta(-\|\tilde{\vec{x}}_i^\nu - \tilde{\vec{x}}_j^\nu\|_\infty) = 1$.
- 173 (2) dissimilar if $\Theta(-\|\tilde{\vec{x}}_i^\nu - \tilde{\vec{x}}_j^\nu\|_\infty) = 0$.

174 This point of view leads to the idea of proposing an approximation of $\mathcal{PP}^{(\nu)}$
 175 for $\varepsilon > 0$ by replacing $\Theta(\varepsilon - \|\vec{x}_i^\nu - \vec{x}_j^\nu\|_\infty)$ by $\Theta(-\|\tilde{\vec{x}}_i^\nu - \tilde{\vec{x}}_j^\nu\|_\infty)$ in Eq. (4):

176 **Definition 1.** Let $\varepsilon > 0$. The approximations $\tilde{\mathcal{P}}\mathcal{P}^{(\nu)}$ and $\tilde{DET}^{(\mu)}$ of $\mathcal{P}\mathcal{P}^{(\nu)}$
 177 and $DET^{(\mu)}$ respectively are defined as

$$\tilde{\mathcal{P}}\mathcal{P}^{(\nu)} := \sum_{i,j=1}^{N-\nu+1} \Theta(-\|\tilde{x}_i^\nu - \tilde{x}_j^\nu\|_\infty),$$

$$\tilde{DET}^{(\mu)} := \frac{\mu \cdot \tilde{\mathcal{P}}\mathcal{P}^{(\mu)} - (\mu - 1) \cdot \tilde{\mathcal{P}}\mathcal{P}^{(\mu+1)}}{\tilde{\mathcal{P}}\mathcal{P}^{(1)}}.$$

178 The crucial difference between $\mathcal{P}\mathcal{P}^{(\nu)}$ and $\tilde{\mathcal{P}}\mathcal{P}^{(\nu)}$ is that for the latter the
 179 similarity threshold is zero. In this case $\tilde{\mathcal{P}}\mathcal{P}^{(\nu)}$ can be calculated algorithmically
 180 by applying Theorem 1 for $X = \tilde{x}^\nu$ (rather than $X = x^\nu$). Then $\tilde{DET}^{(\mu)}$ simply
 181 utilizes $\tilde{\mathcal{P}}\mathcal{P}^{(\nu)}$ for $\nu = 1, \mu, \mu + 1$ in Theorem 2.

182 At this point, we emphasize that the approximation method and resulting
 183 approximation errors are based on the discretization only. Once we have discretized
 184 the data and use a threshold that is zero, we apply the results from
 185 Sec. 4 in order to calculate the RQA measures efficiently. Quantifying the discretized
 186 data with the use of a recurrence plot will lead to the exact same result.
 187 An example of a discretization is illustrated in Fig. 1.

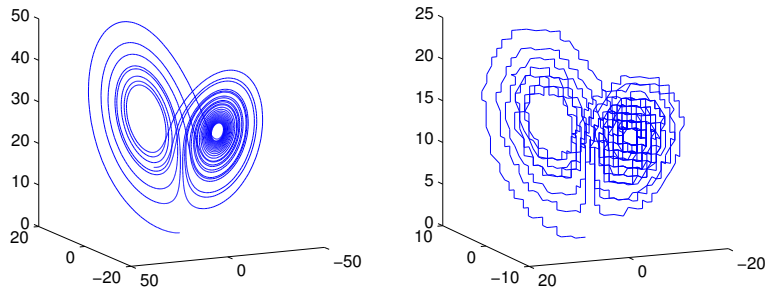


Figure 1: The Lorenz attractor (left) from Eq. (12) and its discretization (right) for grid size parameter $\delta = 2$.

188 5.2. Investigation of the approximation method

189 We explore the phase space discretization from Sec. 5.1 and its impact on
 190 the approximation of $\mathcal{P}\mathcal{P}^{(\nu)}$. Recall that we formulated the approximation
 191 procedure as a classification problem.

192 Denote by $(x, y) \sim C(S, T)$ the situation that x and y are classified as
 193 belonging to class S where they are in fact in class T . Then, if S means ‘similar’,
 194 there are four classification situations (compare with Fig. 2), namely

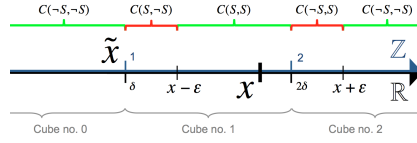


Figure 2: Classification situations for $x \in [1.5\delta, 2\delta)$ and $\delta = 2\varepsilon$. In this one-dimensional case, the hypercubes are simply intervals in \mathbb{R} . Here, $\tilde{x} = 1$ and thus x belongs to the cube no. 1. For $y \in \mathbb{R}$, in fact x and y are similar if $y \in [x - \varepsilon, x + \varepsilon]$, hence x and y are not classified correctly if $y \in [\delta, x - \varepsilon)$ or $y \in [2\delta, x + \varepsilon]$.

$$\begin{aligned}
(x, y) \sim C(S, S) &\Leftrightarrow \tilde{x} = \tilde{y} \quad \text{and} \quad \|x - y\|_\infty \leq \varepsilon. \\
(x, y) \sim C(\neg S, \neg S) &\Leftrightarrow \tilde{x} \neq \tilde{y} \quad \text{and} \quad \|x - y\|_\infty > \varepsilon. \\
(x, y) \sim C(S, \neg S) &\Leftrightarrow \tilde{x} = \tilde{y} \quad \text{and} \quad \|x - y\|_\infty > \varepsilon. \\
(x, y) \sim C(\neg S, S) &\Leftrightarrow \tilde{x} \neq \tilde{y} \quad \text{and} \quad \|x - y\|_\infty \leq \varepsilon.
\end{aligned}$$

195 For \vec{x}^ν we conclude the following observations.

- 196 1. If for each pair $(\vec{x}_i^\nu, \vec{x}_j^\nu) \sim C(S, S)$ or $(\vec{x}_i^\nu, \vec{x}_j^\nu) \sim C(\neg S, \neg S)$, then clearly
197 $\tilde{\mathcal{P}}\mathcal{P}^{(\nu)} = \mathcal{P}\mathcal{P}^{(\nu)}$. However,
198 2. if $(\vec{x}_i^\nu, \vec{x}_j^\nu) \sim C(\neg S, S)$, the similarity of $(\vec{x}_i^\nu, \vec{x}_j^\nu)$ increases $\mathcal{P}\mathcal{P}^{(\nu)}$, but not
199 $\tilde{\mathcal{P}}\mathcal{P}^{(\nu)}$; and
200 3. if $(\vec{x}_i^\nu, \vec{x}_j^\nu) \sim C(S, \neg S)$, the dissimilarity of $(\vec{x}_i^\nu, \vec{x}_j^\nu)$ increases $\tilde{\mathcal{P}}\mathcal{P}^{(\nu)}$, but
201 not $\mathcal{P}\mathcal{P}^{(\nu)}$.

202 Therefore these two types of errors satisfy a mutual cancelling property, and if
203 the number of $C(\neg S, S)$ -errors equals the number of $C(S, \neg S)$ -errors, then even
204 $\tilde{\mathcal{P}}\mathcal{P}^{(\nu)} = \mathcal{P}\mathcal{P}^{(\nu)}$ follows.

205 From these considerations we establish the choice of $\delta = 2\varepsilon$.

206 5.2.1. The discretization parameter δ

207 The grid size δ of the discretization determines which elements are classified
208 as similar and thus has to be chosen carefully. If we make no further assumptions
209 to the data, by intuition $\delta = 2\varepsilon$ is a reasonable choice since the similarity
210 diameter in phase space is 2ε , and moreover the different error zones have exactly
211 the same measure (see Fig. 2). This also means that $\delta = 2\varepsilon$ is optimal and
212 leads to nearly zero approximation error if the values of the time series x are
213 independent uniformly distributed (on an appropriate interval). Note that $\varepsilon > 0$
214 was supposed implicitly since $\delta > 0$ is required in Eq. (8). If $\varepsilon = 0$, then no
215 discretization is applied, and in fact not necessary since from Theorem 1 follows
216 that the exact quantity $\mathcal{P}\mathcal{P}^{(\nu)}$ can be calculated efficiently. Let us now discuss
217 the algorithmic details.

218 *5.2.2. Algorithms*

219 The previous findings are used to provide algorithms for the calculation of
 220 the approximations from Definition 1; and in case of $\varepsilon = 0$ for fast calculation of
 221 the exact measures $\mathcal{PP}^{(\nu)}$ and $DET^{(\mu)}$. Since the methods for fast processing of
 222 the approximations and the exact terms are identical, for $\varepsilon = 0$ we now denote
 223 $\tilde{x}^\nu := \tilde{x}^\nu$ and state algorithms for $\tilde{\mathcal{PP}}^{(\nu)}$ and $\tilde{DET}^{(\mu)}$, given an arbitrary $\varepsilon \geq 0$.

224 As already observed in Sec. 4.1 it is enough to find the histogram h_X of
 225 the (discretized) sequence of trajectory embedding vectors $X := \tilde{x}^\nu$, since then
 226 $\tilde{\mathcal{PP}}^{(\nu)}$ is given by

$$\tilde{\mathcal{PP}}^{(\nu)} = \sum_{\tilde{y} \in Y} (h_X(\tilde{y}))^2, \quad (9)$$

227 where Y is again the set of unique members of X . Technically, this may be
 228 achieved by assigning unique identifiers to the elements in X , i.e., we are inter-
 229 ested in integers $J_1, \dots, J_{N-\nu+1}$, such that

$$\tilde{x}_i^\nu = \tilde{x}_j^\nu \Leftrightarrow J_i = J_j \quad \text{for all } i, j,$$

230 and charge the histogram of these identifiers (compare with Algorithm 1). The
 231 calculation of $\tilde{DET}^{(\mu)}$ is presented in Algorithm 2. Finally, the efficiency of
 232 these procedures is argued in section 5.2.3.

233 Recall the designations. For more clarity, we eliminate the vector arrows in
 234 the algorithms, i.e., $x := \vec{x}$ is the trajectory of length N , $\varepsilon \geq 0$ is the similarity
 235 threshold, μ the minimum diagonal line length, ν is the trajectory embedding
 236 dimension and $x^\nu := \vec{x}^\nu$ is the matrix that consists of the rows $x_j^\nu := \vec{x}_j^\nu$,
 237 $j = 1, \dots, N - \nu + 1$. We emphasize that the algorithm is not restricted to
 238 one-dimensional trajectories x , provided appropriate implementation. In Sec. 6
 239 we provide MATLAB[®] code that handles multi-dimensional data.

Algorithm 1 Fast calculation of $\tilde{\mathcal{PP}}^{(\nu)}$ (or $\mathcal{PP}^{(\nu)}$ if $\varepsilon = 0$)

```

1: procedure PPAPPROX( $x, \varepsilon, \nu$ )
2:   if  $\varepsilon = 0$  then                                     ▷ No discretization, method is exact.
3:      $\tilde{x} \leftarrow x$ 
4:   else                                               ▷ Discretization of phase space, Eq. (8).
5:      $\delta \leftarrow 2\varepsilon$ 
6:      $\tilde{x} \leftarrow \Phi_\delta(x)$ 
7:   end if
8:    $\tilde{x}^\nu \leftarrow \text{apply\_trajectory\_embedding}(\tilde{x}, \nu)$ 
9:    $J = (J_1, \dots, J_{N-\nu+1}) \leftarrow \text{find\_unique\_row\_IDs}(\tilde{x}^\nu)$ 
10:   $h \leftarrow \text{histogram}(J)$ 
11:   $\tilde{\mathcal{PP}}^{(\nu)} \leftarrow \sum_i h_i^2$ 
12: end procedure

```

240 *5.2.3. Complexity analysis*

241 Denote by \mathcal{O}_c and \mathcal{O}_s the computational and space complexity respectively.

242 **Theorem 3.** *Let ν and $\mu \in \mathbb{N}$ be fixed choices of the trajectory embedding*
 243 *dimension and the minimum diagonal line length, respectively.*

Algorithm 2 Fast calc. of $D\tilde{E}T^{(\mu)}$ (or $DET^{(\mu)}$ if $\varepsilon = 0$)

```

1: procedure DETAPPROX( $x, \varepsilon, \mu$ )
2:    $\mathcal{PP}^{(1)} \leftarrow \text{PPapprox}(x, \varepsilon, 1)$ 
3:    $\mathcal{PP}^{(\mu)} \leftarrow \text{PPapprox}(x, \varepsilon, \mu)$ 
4:    $\mathcal{PP}^{(\mu+1)} \leftarrow \text{PPapprox}(x, \varepsilon, \mu + 1)$ 
5:    $D\tilde{E}T^{(\mu)} \leftarrow (\mu \cdot \mathcal{PP}^{(\mu)} + (\mu - 1) \cdot \mathcal{PP}^{(\mu+1)}) / \mathcal{PP}^{(1)}$ 
6: end procedure

```

- 244 (i) The complexity classes of the approximations $\tilde{\mathcal{PP}}^{(\nu)}$ and $D\tilde{E}T^{(\mu)}$ are $\mathcal{O}_c(N \log(N))$
245 and $\mathcal{O}_s(N)$.
- 246 (ii) If $\varepsilon = 0$, then the exact terms $\mathcal{PP}^{(\nu)}$ and thus the exact RQA-measures
247 RR and $DET^{(\mu)}$ are in the complexity classes $\mathcal{O}_c(N \log(N))$ and $\mathcal{O}_s(N)$,
248 given an arbitrary phase space norm $\|\cdot\|$.

249 **PROOF.** We investigate the complexity of Algorithm 1. The complexity class of
250 Algorithm 2 is clearly identical.

251 (i) It is easy to verify that the operations in lines 2-8 are in $\mathcal{O}_c(N)$ and
252 $\mathcal{O}_s(N)$. The main cost is taken by line 9. One way to find unique identifiers for
253 the rows of \tilde{x}^ν is based on sorting the rows lexicographically. Provided a one
254 dimensional sorting algorithm that operates in $\mathcal{O}_c(N \log(N))$ and $\mathcal{O}_s(N)$, e.g.,
255 QuickSort, the computational complexity of sorting the rows lexicographically
256 is in $\mathcal{O}_c(N \nu \log(N))$ [21]. Then incrementally each row \tilde{x}_i^ν is assigned to an ID
257 J_i in $\mathcal{O}_c(1)$, leading to a complexity of $\mathcal{O}_c(N)$ for the assignment step. Since
258 ν is constant, the overall complexity in line 9 is $\mathcal{O}_c(N \log(N))$. In line 10 it
259 is enough to incrementally count equal entries in J , giving $\mathcal{O}_c(N)$. Finally the
260 complexity in line 11 is $\mathcal{O}_c(N)$ since $n \leq N$, where n is the length of the vector
261 h . Altogether the dominating complexity classes are $\mathcal{O}_c(N \log(N))$ and $\mathcal{O}_s(N)$.

262 (ii) Let $\varepsilon = 0$. Determine $\mathcal{PP}^{(1)}$ using Algorithm 1 and set $RR = \mathcal{PP}^{(1)} / N^2$.
263 Compute $DET^{(\mu)}$ using Algorithm 2. By Theorem 1 and 2 these expressions
264 coincide with the exact RQA-measures. As already mentioned in Sec. 4.2, if
265 $\varepsilon = 0$, then the identities hold for an arbitrary phase space norm since each
266 norm only indicates whether two elements in phase space are equal. The claim
267 on the complexity classes is proven in the first part. \square

268 We remark that sorting the rows lexicographically is not the only possibility.
269 One could, for instance, use a hash function that maps the embedding vectors
270 to \mathbb{R} in order to get the identifiers for the embedding vectors and then apply a
271 simple one-dimensional sorting algorithm to find the histogram incrementally.
272 However, such hash functions do not guarantee unique identifiers since they are
273 not injective in general.

274 5.2.4. Worst case error

275 As shown in Theorem 3, if $\varepsilon = 0$, then $\mathcal{PP}^{(\nu)}$ can be calculated exactly and
276 efficiently. If $\varepsilon > 0$, the approximation $\tilde{\mathcal{PP}}^{(\nu)}$ of $\mathcal{PP}^{(\nu)}$ satisfies the following
277 estimates.

278 **Theorem 4.** *Let $\varepsilon > 0$ and $\delta = 2\varepsilon$. In d -dimensional phase space it holds*

$$\frac{1}{2^{d\nu}} \mathcal{P}\mathcal{P}^{(\nu)} \leq \tilde{\mathcal{P}}\mathcal{P}^{(\nu)} \leq 2^{d\nu} \mathcal{P}\mathcal{P}^{(\nu)}.$$

279 **PROOF.** Denote $m = d\nu$. The lower bound is reached if the number of $C(-S, S)$ -
 280 errors is maximal. Let \vec{y} be a vertex of the discretization lattice. In m -
 281 dimensional space there are 2^m adjoint hypercubes surrounding \vec{y} . Hence it is
 282 possible to place 2^m points \vec{x}_i , each in another cube, such that $\|\vec{y} - \vec{x}_i\|_\infty \leq \varepsilon/2$
 283 for all i . It follows that $\|\vec{x}_i - \vec{x}_j\|_\infty \leq \varepsilon$ for all i, j . Hence each pair (\vec{x}_i, \vec{x}_j)
 284 is similar, but by construction classified as dissimilar if $i \neq j$. In this case we
 285 have $\mathcal{P}\mathcal{P}^{(\nu)} = (2^m)^2$ and $\tilde{\mathcal{P}}\mathcal{P}^{(\nu)} = 2^m$. The argument is finished since placing
 286 additional points only leads to a reduction of the number of $C(-S, S)$ -errors.

287 The upper bound follows in a similar manner by producing errors of type
 288 $C(S, -S)$. □

289 By now the bounds are shown to be existent (hence the theorem is true)
 290 but not that they are sharp. One would have to show that there is a trajectory
 291 whose embedding vectors are constructed as above. For $\nu = 2$ and $d = 1$ an
 292 appropriate trajectory is given by $\vec{x} = (\eta, \eta, -\eta, -\eta, \eta)$, where $\eta < \varepsilon/2$. The four
 293 resulting trajectory embedding vectors of \vec{x} satisfy the above construction. For
 294 general ν and d this becomes more technical, but we think that this investigation
 295 is unnecessary at this point. It is more interesting how the approximation error
 296 behaves empirically.

297 5.2.5. Empirical approximation error

298 As seen in Sec. 5.2.4 the bounds of the approximation error of $\tilde{\mathcal{P}}\mathcal{P}^{(\nu)}$ are
 299 rather large and monotonic in ν . However, the constructions given in the proof
 300 of Theorem 4 to reach these bounds are very specific.

301 In this section we study the approximation errors of $\tilde{\mathcal{P}}\mathcal{P}^{(\nu)}$ and $D\tilde{E}T^{(\mu)}$
 302 empirically. For this sake the relative mean errors of 100 realizations, designed
 303 as follows, are determined. For each experiment the autoregressive process
 304 $\vec{x} = (x_1, \dots, x_N)$, with

$$x_i = ax_{i-1} + b\eta_i, \quad i = 2, \dots, N \tag{10}$$

305 is generated for $N = 1000$ time steps, where $x_1 = 0$, a, b are fixed values
 306 that are chosen randomly independent uniformly distributed on $[0, 1]$ and η is
 307 a vector of Gaussian white noise. Then the approximations are determined by
 308 the algorithms from section 5.2.2 and the exact quantities $\mathcal{P}\mathcal{P}^{(\nu)}$ and $DET^{(\mu)}$
 309 are calculated by the classical method in order to specify the accuracy of the
 310 approximations. The results are illustrated in Fig. 3 for several combinations
 311 of ν (resp. μ) and ε , where the height of the bars corresponds to the mean
 312 error and the color of the bars corresponds to the value $\mathcal{P}\mathcal{P}^{(\nu)}$ and $DET^{(\mu)}$,
 313 respectively. It is customary to select ε as a few percent of the phase space
 314 diameter $[1, 22]$, which in this case is given by $\text{range}(\vec{x}) = \max(\vec{x}) - \min(\vec{x})$.

315 We observe that the approximation errors are basically increasing in ν (resp.
316 μ) and ε . However, most of the combinations of ν (resp. μ) and ε have little
317 relevance. First, if ε is small and ν (resp. μ) is large, the probability to find
318 recurrences is low. Consequently the bars in Fig. 3 (a) are of deep blue color.
319 Therefore the low error in this area is an artefact. Conversely, if ν (resp. μ)
320 is small and ε is large, too many recurrences are found, resulting in red colors.
321 Reasonable choices of ν (resp. μ) and ε are indicated by colors in the range
322 from blue-green to orange-red in Fig. 3 (a).

323 As an example, assume that we want to determine the recurrence rate and
324 the determinism of the trajectory \vec{x} . For the calculation of the determinism, a
325 minimal line length of $\mu = 2$ is sufficient, because for the autoregressive process
326 we do not expect much effect of tangential motion or sampling [1]. Then for
327 all sensible values of ε , i.e., from 0 to 8 percent of the range, we obtain mean
328 approximation errors below 1.4% for the recurrence rate and below 2.7% for the
329 determinism.

330 It should be noticed that we have investigated one-dimensional trajectories
331 \vec{x} that are not reconstructed by time series embedding. However, the trajectory
332 embedding of dimension ν can also be imagined as time series embedding if we
333 postulate that \vec{x} is the time series and \vec{x}^ν is the trajectory, which is obtained
334 from \vec{x} by time series embedding with time delay 1 and embedding dimension
335 ν . Then Fig. 3 (a) reflects the approximation errors of the recurrence rate
336 of \vec{x}^ν , which is given by $\mathcal{P}\mathcal{P}^{(\nu)}/(N - \nu + 1)^2$. The essence of this technical
337 point of view is that the approximation errors increase if the dimension of the
338 trajectory increases. We also observe this in the experiment from Sec. 6 for the
339 3-dimensional Lorenz attractor, see Tab. 2.

340 6. Execution Time of Algorithm 1

341 We compare the execution times of $\mathcal{P}\mathcal{P}$ and its approximation $\tilde{\mathcal{P}}\tilde{\mathcal{P}}$ on a
342 consumer computer (2.3 GHz Intel Core i7 quad core processor, 16 GB 1600 MHz
343 DDR3 RAM). Since execution times do not only depend on the algorithm, but
344 also on the implementation, we provide MATLAB[®] code. Note that, however,
345 this code uses standard MATLAB[®] routines and may be strongly optimized by
346 the MATLAB[®] compiler.

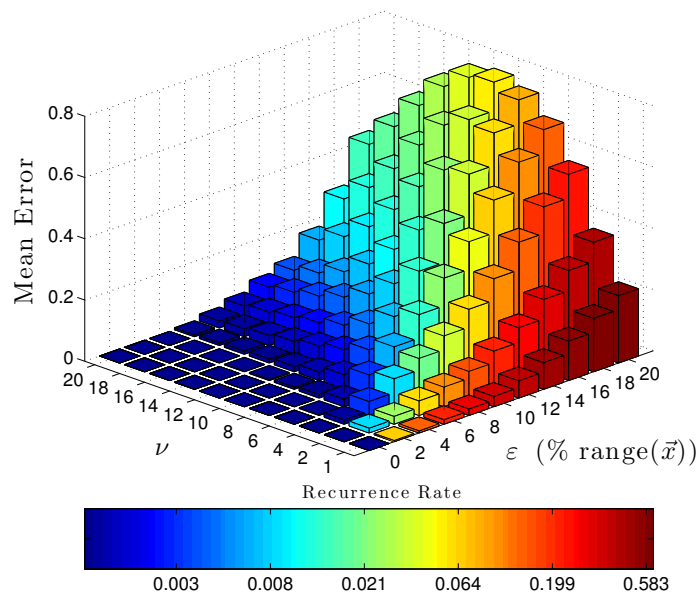
We evaluate two systems, the autoregressive process

$$x_1 = 0, \quad x_i = 0.57x_{i-1} + 0.24\eta_i, \quad i = 2, \dots, 100.000.000 \quad (11)$$

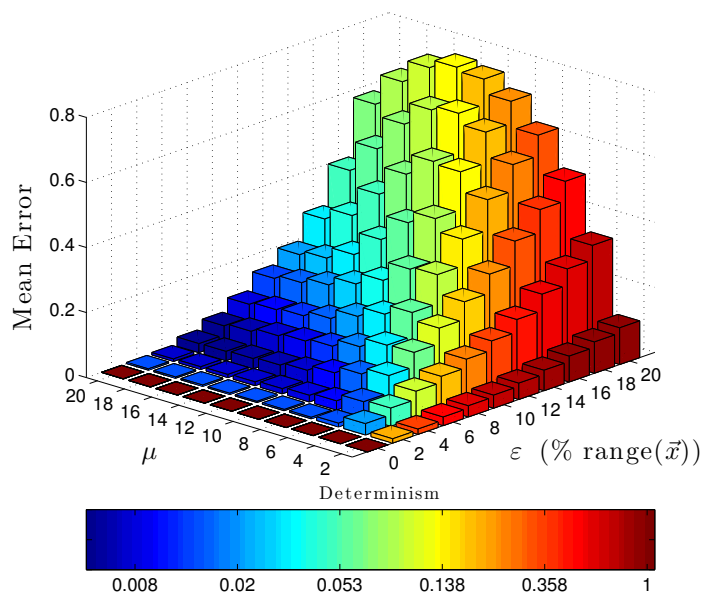
and the well known 3-dimensional Lorenz system (see Fig. 1)

$$\dot{x} = a(y - x), \quad \dot{y} = x(b - z) - y, \quad \dot{z} = xy - cz \quad (12)$$

347 for the parameters $a = 10, b = 28, c = 8/3$. Then these systems are truncated
348 according to the values of N as listed in the tables of results, Tab. 1 and 2, and
349 processed by the routines. The threshold ε was chosen for each N separately
350 as 7% of the phase space diameter and no embedding is applied, i.e. $m = 1$ in
351 the following MATLAB[®] function.



(a) Approximation error of $\tilde{RR}^{(\nu)}$



(b) Approximation error of $\tilde{DET}^{(\mu)}$

Figure 3: Relative mean errors obtained from 100 autoregressive process realizations. The bar color in Figure (a) indicates the value of the exact recurrence rate $RR^{(\nu)} = \mathcal{P}\mathcal{P}^{(\nu)} / (N - \nu + 1)^2$ of the embedded trajectory \tilde{x}^ν . The bar color in Figure (b) reflects the exact determinism $DET^{(\mu)}$ of the trajectory \tilde{x} , given a minimum diagonal line length μ .

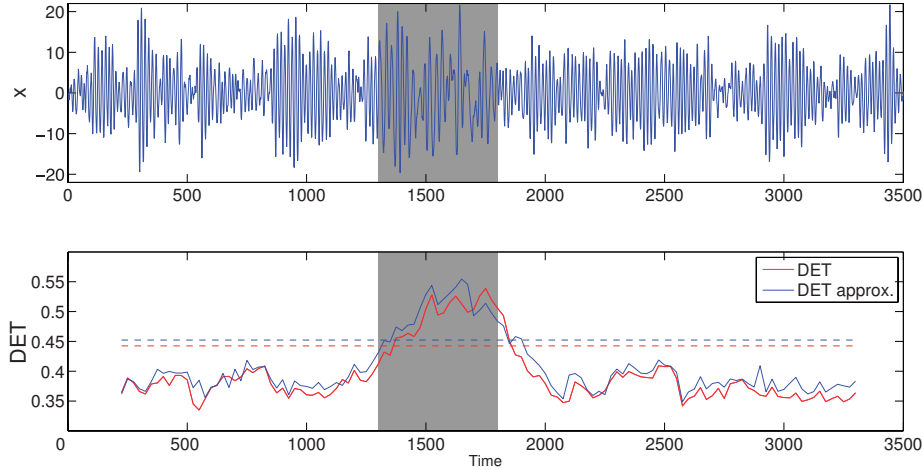


Figure 4: Example from the transition experiment. The system of the upper plot is generated as described in Sec. 7.2. The lower graphic shows the window-wise determinism sequence \mathcal{D} (red) and its approximation $\tilde{\mathcal{D}}$ (blue). The dashed lines are the confidence levels.

```

352 MATLAB® code for  $\tilde{\mathcal{P}}\mathcal{P}$ .
353 function pp = PPapprox( x, eps, m)
354 [N,d] = size(x);
355 if eps > 0                                % discretize if eps > 0
356     x = floor(x/(2*eps));
357 end
358 X = zeros(N-m+1,d*m);                      % apply trajectory embedding
359 for i = 1:m
360     X(:,d*(i-1)+1:d*i) = x(i:N-(m-i),:);
361 end
362 [u,~,iu] = unique(X,'rows');               % find row ID's iu
363 h = hist(iu,size(u,1));                    % find histogram of row ID's
364 pp = sum(h.^2);
365 % end of function PPapprox

366 MATLAB® code for  $\mathcal{P}\mathcal{P}$ .
367 function pp = PP( x, eps)
368 R = pdist2(x,x,'chebychev') <= eps;       % calculate recurrence plot
369 pp = nnz(R);                               % count non zeros
370 % end of function PP

```

371 Since the available memory on the computer was 12 GB, we limited the data
372 size for the exact measure $\mathcal{P}\mathcal{P}$. Indeed a single recurrence plot for $N = 40.000$
373 consumes about 12 GB of RAM, provided double precision and no storage op-
374 timization. For $N = 100.000$ even about 75 GB of memory would be required.

N	Execution Time \mathcal{PP} (sec.)	Execution Time $\tilde{\mathcal{PP}}$ (sec.)	Approximation Error
100	0.0552	0.0005	0.0275
1.000	0.0078	0.0005	0.0104
10.000	0.9058	0.0018	0.0098
20.000	3.7314	0.0158	0.0098
30.000	8.3865	0.0233	0.0096
35.000	13.7078	0.0131	0.0092
100.000	-	0.0169	-
1.000.000	-	0.1912	-
10.000.000	-	2.2587	-
100.000.000	-	28.5899	-

Table 1: Mean execution times obtained from 10 realizations of the Autoregressive process (11). The approximation error is again the mean over the relative errors $|\mathcal{PP} - \tilde{\mathcal{PP}}|/\mathcal{PP}$.

N	Execution Time \mathcal{PP} (sec.)	Execution Time $\tilde{\mathcal{PP}}$ (sec.)	Approximation Error
100	0.0513	0.0009	0.0471
1.000	0.0077	0.0006	0.3655
10.000	0.9071	0.0052	0.2885
20.000	3.7200	0.0074	0.2646
30.000	8.2962	0.0117	0.2746
100.000	-	0.0396	-
1.000.000	-	0.3645	-

Table 2: Mean execution times obtained from 10 realizations of the Lorenz system (12). The approximation error is again the mean over the relative errors $|\mathcal{PP} - \tilde{\mathcal{PP}}|/\mathcal{PP}$.

375 The results give numerical evidence for the complexity we have proved in The-
 376 orem 3 and reflect the large difference between $\mathcal{O}(N^2)$ and $\mathcal{O}(N \log(N))$ for
 377 increasing N . For example the ratio of execution times for the autoregressive
 378 process with $N = 35.000$ is about 1.046. Moreover, the algorithm is very fast for
 379 extreme large data and the approximation error decreases slightly with growing
 380 N . In Tab. 2 the small approximation error for $N = 100$ is due to the short
 381 and hence almost linear attractor. As expected, the other errors of the Lorenz
 382 experiment are higher since the attractor is 3-dimensional.

383 7. Application to transition detection

384 7.1. Introduction to the problem

385 Assume that we are given a time series or a stream $x = (x_1, x_2, x_3, \dots)$ which
 386 changes its dynamics at unknown time segments. It has been shown that the
 387 determinism $DET^{(\mu)}$ is able to find these periods [5, 6, 23]. For this, the time
 388 series is analyzed window-wise for a window size w and step size s , leading to a

389 sequence \mathcal{D} of determinism-values. More precisely, $\mathcal{D}(j)$ contains the determinism
390 of the sub-sequence $(x_{s \cdot j}, \dots, x_{s \cdot j + w - 1})$, $j = 1, 2, 3, \dots$. A transition in the
391 dynamics is indicated when the system leaves its typical dynamical behaviour,
392 in this case its typical range of the window-wise determinism values [6]. The
393 bounds of this range are referred to as confidence levels. An example of a graph
394 of \mathcal{D} is illustrated as red line in Fig. 4. In the gray marked area the system
395 from the upper plot changes its dynamics (details in Sec. 7.2) and consequently
396 \mathcal{D} exceeds its upper confidence bound, which is represented by the dashed red
397 line.

398 In this section we compare our proposed approximation $D\tilde{E}T^{(\mu)}$ to the exact
399 measure $DET^{(\mu)}$ for the problem of identifying transition times. Again, we
400 consider a minimal line length of $\mu = 2$. It remains to select ε . For each window
401 ε is determined separately such that the recurrence rate is a small fraction,
402 e.g., 0.1 [6]. This leads to a constant (in time index i) denominator in Eq. (2)
403 accentuating the behaviour of the changes in $P(l)$.

404 7.2. Design of the experiment with autoregressive data

405 The experiment is inspired by [6]. We evaluate 100 realizations employing
406 autoregressive processes of order 2,

$$x_i = ax_{i-1} - bx_{i-2} + c\eta_i.$$

407 The test time series is initially generated for $x_1 = x_2 = 0$ and $a = 1.8, b =$
408 $0.972, c = 0.64$ for 1300 time steps. Then the parameters change for a period of
409 500 time steps to $a = 1.85, b = 0.917, c = 0.76$. Finally the system returns to
410 the initial parameters and stops at time step 3500. The resulting time series x
411 is then analysed for a window size $w = 400$ and step size $s = 25$.

412 In the exact case \mathcal{D} contains the values of $DET^{(2)}$, where ε is chosen such
413 that the recurrence rate $\mathcal{P}\mathcal{P}^{(1)}/w^2$ is 0.1. In the approximative case $\tilde{\mathcal{D}}$ contains
414 the values of $D\tilde{E}T^{(2)}$, where ε is chosen such that the approximate recurrence
415 rate $\tilde{\mathcal{P}}\tilde{\mathcal{P}}^{(1)}/w^2$ is 0.1.

416 In order to find the upper confidence level, we assume that the system with
417 initial parameters is observed for $N = 100\,000$ time steps and the distribution
418 of the (approximate) determinism values for the windows is charged. We choose
419 as transition level the 99.95%-quantile of those distributions, leading to a con-
420 fidence level of 0.4425 for $DET^{(2)}$ and 0.4523 for $D\tilde{E}T^{(2)}$. For the evaluation
421 the time points of exceeding and falling below these levels are compared to
422 the actual transition time at 1300 and 1800. The results reveal that our fast
423 approximation performs as well as the slow exact method (Tab. 3).

424 7.3. Transitions in the logistic map

We briefly illustrate that the approximate determinism $D\tilde{E}T$ is also able to
find transitions in the logistic map

$$x_1 = 0.7, \quad x_{i+1} = ax_i(1 - x_i),$$

Measure	Left transition error	Right transition error
$DET^{(2)}$	61.25	64.75
$\tilde{DET}^{(2)}$	85.00	45.50

Table 3: Mean transition errors obtained from 100 realizations as described in Sec. 7.2. The left/right transition error is defined as the absolute deviation from time index 1300/1800.

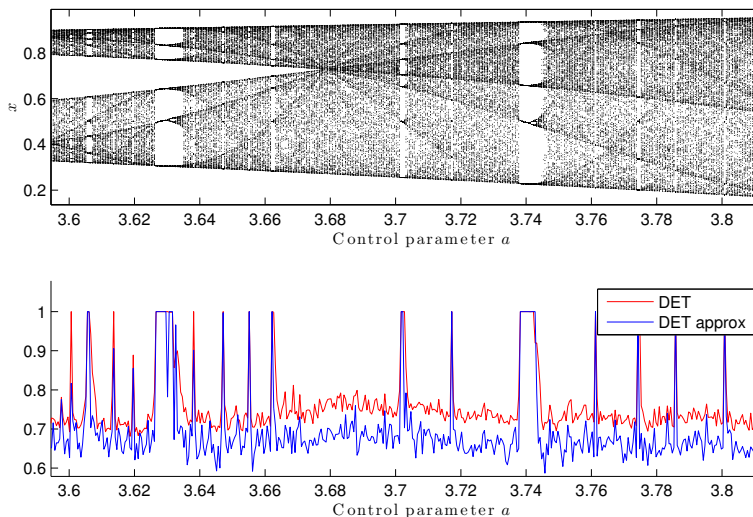


Figure 5: Bifurcation diagram of the logistic map and its dynamics. We observe multiple chaos-period transitions that are found by both measures, DET (red) and \tilde{DET} (blue).

425 with control parameter a in the range $[3.6, 3.8]$. In the experiment we observed
426 that the quality of the approximation is sensitive to ε . We found that a rather
427 small threshold is beneficial. More precisely, we selected ϵ for each a separately
428 such that the recurrence rate resp. the approximate recurrence rate is 0.01.
429 Fig. 5 confirms that \tilde{DET} has the capability to find dynamical transitions.

430 8. Other RQA measures

431 Using $\mathcal{PP}^{(\nu)}$ it is possible to specify identities for other diagonal line based
432 RQA-measures. Detailed analysis of those is out of the scope of this work, but
433 we briefly state the formulas in this section. In the following equations the left
434 hand side is the classical definition and the right hand side is the identity in
435 terms of $\mathcal{PP}^{(\nu)}$. As before, μ denotes the minimum diagonal line length, the
436 phase space norm is $\|\cdot\|_\infty$ and the LOI is included unless otherwise stated.

437 For the ratio $RATIO^{(\mu)}$ between $DET^{(\mu)}$ and RR , we get

$$N^2 \frac{\sum_{l \geq \mu} lP(l)}{\left(\sum_{l \geq 1} lP(l)\right)^2} = N^2 \frac{\mu \mathcal{P}\mathcal{P}^{(\mu)} - (\mu - 1)\mathcal{P}\mathcal{P}^{(\mu+1)}}{\left(\mathcal{P}\mathcal{P}^{(1)}\right)^2}.$$

438 Due to Eq. (7), the averaged diagonal line length $L^{(\mu)}$ is given by

$$\frac{\sum_{l \geq \mu} lP(l)}{\sum_{l \geq \mu} P(l)} = \frac{\mu \mathcal{P}\mathcal{P}^{(\mu)} - (\mu - 1)\mathcal{P}\mathcal{P}^{(\mu+1)}}{\mathcal{P}\mathcal{P}^{(\mu)} - \mathcal{P}\mathcal{P}^{(\mu+1)}},$$

439 and the length of the longest diagonal line L_{\max} (excluding the LOI , i.e., $P(N) :=$
440 0), determined by

$$\max\{l \mid P(l) \neq 0\} = \min\{\nu \mid \mathcal{P}\mathcal{P}^{(\nu)} = N - \nu + 1\} - 1,$$

441 can be found by binary search in $\mathcal{O}(\log(N))$ iterations since $\nu \mapsto \mathcal{P}\mathcal{P}^{(\nu)}$ is
442 monotonically decreasing.

443 Finally we should remember that these expressions can be calculated ex-
444 actly and efficiently if $\varepsilon = 0$; and in case of $\varepsilon > 0$ the measures can be ap-
445 proximated efficiently by replacing $\mathcal{P}\mathcal{P}$ by $\tilde{\mathcal{P}}\tilde{\mathcal{P}}$. In both cases Algorithm 1
446 determines the pairwise proximity measures efficiently. For \tilde{L}_{\max} the resulting
447 computational complexity is $\mathcal{O}(N \log^2(N))$. All other approximative measures
448 are in $\mathcal{O}(N \log(N))$, whereas the complexity of the classical measures is $\mathcal{O}(N^2)$
449 [11].

450 9. Conclusions

451 We have shown that the recurrence rate and many diagonal line based RQA-
452 measures can be calculated efficiently, i.e., in $\mathcal{O}(N \log(N))$ if the similarity
453 threshold ε is zero. For the case $\varepsilon > 0$ we have introduced approximations
454 to these measures that are based on phase space discretization and a relation
455 between the histogram of the diagonal line lengths $P(l)$ and the introduced
456 pairwise proximity measures of trajectory embeddings. For small embedding
457 dimension ν or minimum diagonal line length μ the proposed approximations
458 are very close to the exact quantities in our experiments with one-dimensional
459 data, while execution times and memory consumption are significantly lower.
460 However, we recommend to compare the approximations to the exact measures
461 on the data of interest before doing serious RQA with it. In particular, if the
462 trajectory is multi-dimensional the approximation error may increase. We also
463 recommend to keep ε as small as possible since it determines the grid size of the
464 discretization. Of course a small grid size leads to a gentle discretization and
465 hence to low approximation errors.

466 In future work it should be investigated whether data-adopted discretization
467 lattices are able to improve the approximation accuracy. It is also interesting
468 if there are conditions under which the ratio $D\tilde{E}T(\vec{x})/DET(\vec{x})$ stays stable
469 (nearly constant) in changing \vec{x} . Of course, if the approximation error is small
470 this stability is present, but if the error is large, this stability would still allow

471 us to compare dynamics rather than determine dynamics, which is sufficient for
472 many applications, e.g. transition detection.

473 References

- 474 [1] N. Marwan, M. C. Romano, M. Thiel, J. Kurths, Recurrence Plots for the
475 Analysis of Complex Systems, *Physics Reports* 438 (5–6) (2007) 237–329.
476 doi:10.1016/j.physrep.2006.11.001.
- 477 [2] C. L. Webber, Jr., N. Marwan, Recurrence Quantification Analysis –
478 Theory and Best Practices, Springer, Heidelberg, 2015. doi:10.1007/
479 978-3-319-07155-8.
- 480 [3] C. L. Webber, Jr., N. Marwan, A. Facchini, A. Giuliani, Simpler methods
481 do it better: Success of Recurrence Quantification Analysis as a general
482 purpose data analysis tool, *Physics Letters A* 373 (2009) 3753–3756. doi:
483 10.1016/j.physleta.2009.08.052.
- 484 [4] N. Marwan, J. Kurths, Comment on “stochastic analysis of recurrence plots
485 with applications to the detection of deterministic signals” by rohde et
486 al. [*physica d* 237 (2008) 619–629], *Physica D* 238 (16) (2009) 1711–1715.
487 doi:10.1016/j.physd.2009.04.018.
- 488 [5] A. Facchini, C. Mocenni, N. Marwan, A. Vicino, E. B. P. Tiezzi, Non-
489 linear time series analysis of dissolved oxygen in the Orbetello Lagoon
490 (Italy), *Ecological Modelling* 203 (3–4) (2007) 339–348. doi:10.1016/j.
491 ecolmodel.2006.12.001.
- 492 [6] N. Marwan, S. Schinkel, J. Kurths, Recurrence plots 25 years later – gaining
493 confidence in dynamical transitions, *Europhysics Letters* 101 (2013) 20007.
494 doi:10.1209/0295-5075/101/20007.
- 495 [7] S. Spiegel, J.-B. Jain, S. Albayrak, A Recurrence Plot-Based Distance Mea-
496 sure, Springer, Cham, 2014, pp. 1–15.
- 497 [8] Serrà, M. Müller, P. Grosche, J. L. Arcos, Unsupervised Music Structure
498 Annotation by Time Series Structure Features and Segment Similarity,
499 *IEEE Transactions on Multimedia* 16 (5) (2014) 1229–1240. doi:10.1109/
500 TMM.2014.2310701.
- 501 [9] S. Raiesdana, S. M. R. H. Golpayegani, S. M. P. Firoozabadi, J. M.
502 Habibabadi, On the discrimination of patho-physiological states in epilepsy
503 by means of dynamical measures, *Computers in Biology and Medicine*
504 39 (12) (2009) 1073–1082. doi:10.1016/j.combiomed.2009.09.001.
- 505 [10] J. M. Nichols, S. T. Trickey, M. Seaver, Damage detection using multi-
506 variate recurrence quantification analysis, *Mechanical Systems and Signal*
507 *Processing* 20 (2) (2006) 421–437. doi:10.1016/j.ymsp.2004.08.007.

- 508 [11] T. Rawald, M. Sips, N. Marwan, D. Dransch, Fast Computation of Recur-
509 rences in Long Time Series, Springer, Cham, 2014, pp. 17–29.
- 510 [12] K. Kulkarni, P. Turaga, Recurrence textures for human activity recognition
511 from compressive cameras, 2012, pp. 1417–1420. doi:10.1109/ICIP.2012.
512 6467135.
- 513 [13] G. Varni, G. Dubus, S. Oksanen, G. Volpe, M. Fabiani, R. Bresin,
514 J. Kleimola, V. Välimäki, A. Camurri, Interactive sonification of synchroni-
515 sation of motoric behaviour in social active listening to music with mobile
516 devices, Journal on Multimodal User Interfaces 5 (3–4) (2012) 157–173.
517 doi:10.1007/s12193-011-0079-z.
- 518 [14] T. Rybak, Using GPU to improve performance of calculating recurrence
519 plot, Zeszyty Naukowe Politechniki Białostockiej. Informatyka 6 (2010)
520 77–94.
521 URL [http://www.bogomips.w.tkb.pl/publications/zn-2010-cuda.](http://www.bogomips.w.tkb.pl/publications/zn-2010-cuda.pdf)
522 pdf
- 523 [15] S. Spiegel, S. Albayrak, An order-invariant time series distance measure
524 - position on recent developments in time series analysis, in: Proceedings
525 of 4th International Conference on Knowledge Discovery and Information
526 Retrieval (KDIR), SciTePress, 2012, pp. 264–268.
- 527 [16] S. Spiegel, B.-J. Jain, S. Albayrak, A recurrence plot-based distance mea-
528 sure, Springer Proceedings in Mathematics - Translational Recurrences:
529 From Mathematical Theory to Real-World Applications TO APPEAR.
- 530 [17] N. H. Packard, J. P. Crutchfield, J. D. Farmer, R. S. Shaw, Geometry
531 from a Time Series, Physical Review Letters 45 (9) (1980) 712–716. doi:
532 10.1103/PhysRevLett.45.712.
- 533 [18] N. Marwan, A Historical Review of Recurrence Plots, European Physi-
534 cal Journal – Special Topics 164 (1) (2008) 3–12. doi:10.1140/epjst/
535 e2008-00829-1.
- 536 [19] C. Bandt, A. Groth, N. Marwan, M. C. Romano, M. Thiel, M. Rosen-
537 blum, J. Kurths, Analysis of Bivariate Coupling by Means of Recurrence,
538 Understanding Complex Systems, Springer, Berlin, Heidelberg, 2008, pp.
539 153–182. doi:10.1007/978-3-540-75632-3_5.
- 540 [20] I. P. P. Grassberger, Estimation of the kolmogorov entropy from a chaotic
541 signal, Phys. Rev. A 9 (1-2) (1983) 2591–2593.
- 542 [21] J. Wiedermann, The complexity of lexicographic sorting and searching,
543 in: J. Bečvář (Ed.), Mathematical Foundations of Computer Science 1979,
544 Vol. 74 of Lecture Notes in Computer Science, Springer Berlin Heidelberg,
545 1979, pp. 517–522. doi:10.1007/3-540-09526-8_52.
546 URL http://dx.doi.org/10.1007/3-540-09526-8_52

- 547 [22] S. Schinkel, O. Dimigen, N. Marwan, Selection of recurrence threshold for
548 signal detection, *European Physical Journal – Special Topics* 164 (1) (2008)
549 45–53. doi:10.1140/epjst/e2008-00833-5.
- 550 [23] L. L. Trulla, A. Giuliani, J. P. Zbilut, C. L. Webber, Jr., Recurrence quan-
551 tification analysis of the logistic equation with transients, *Physics Letters*
552 A 223 (4) (1996) 255–260. doi:10.1016/S0375-9601(96)00741-4.

553 **10. Appendix A - Proof of the Determinism Identity**

554 PROOF OF THEOREM 2. Let $\vec{x} = (\vec{x}_1, \dots, \vec{x}_N)$ be a d -dimensional phase space
 555 trajectory ($d \in \mathbb{N}$) of length N and the similarity threshold $\varepsilon \geq 0$ as well as
 556 the minimum diagonal line length $\mu \in \mathbb{N}$ be given. Assume that $\|\cdot\|_\infty$ is the
 557 underlying phase space norm, i.e., the recurrence plot of \vec{x} is given by

$$R_{i,j} = \Theta(\varepsilon - \|\vec{x}_i - \vec{x}_j\|_\infty), \quad i, j = 1, \dots, N,$$

558 and for all $\nu \in \mathbb{N}$ the pairwise proximity measures $\mathcal{PP}^{(\nu)}$ are defined as

$$\mathcal{PP}^{(\nu)} = \sum_{i,j=1}^{N-\nu+1} \Theta(\varepsilon - \|\vec{x}_i^\nu - \vec{x}_j^\nu\|_\infty).$$

559 By definition it holds $\sum_{i,j=1}^N R_{i,j} = \mathcal{PP}^{(1)}$, thus we have to show that the
 560 numerators in Eq. (6) are equal. We show

$$\sum_{l=\mu}^N l \cdot P(l) = \mathcal{PP}^{(\mu)} + (\mu - 1) \cdot (\mathcal{PP}^{(\mu)} - \mathcal{PP}^{(\mu+1)}),$$

561 which gives additional insights into the relation between $P(l)$ and \mathcal{PP} (7). For
 562 this, we define the following index sets.

$$\begin{aligned} I^\mu &= \{(i, j) \mid \Theta(\varepsilon - \|\vec{x}_i^\mu - \vec{x}_j^\mu\|_\infty) = 1\} \\ I_l &= \{(i, j) \mid \sum_{k=0}^{l-1} \Theta(\varepsilon - \|x_{i+k} - x_{j+k}\|_\infty) = \sum_{k=-1}^l \Theta(\varepsilon - \|x_{i+k} - x_{j+k}\|_\infty) = l\} \\ J_l &= \{(i+k, j+k) \mid (i, j) \in I_l, k = 0, \dots, l-1\} \\ I_l^\mu &= I^\mu \cap J_l \end{aligned}$$

563 I^μ contains exactly the index pairs (i, j) such that \vec{x}_i^μ and \vec{x}_j^μ are similar,
 564 thus $\mathcal{PP}^{(\mu)}$ is already determined by $\mathcal{PP}^{(\mu)} = \sum_{(i,j) \in I^\mu} \Theta(\varepsilon - \|\vec{x}_i^\mu - \vec{x}_j^\mu\|_\infty)$.

565 I_l is the set of index pairs (i, j) such that there is a diagonal line of exactly
 566 length l in \mathbf{R} starting at (i, j) , thus $P(l) = |I_l|$.

567 J_l is the set of index pairs (i, j) that exactly cover all diagonal lines of length
 568 l in \mathbf{R} , i.e., $l \cdot P(l) = |J_l|$.

569 Denote $\theta_k = \Theta(\varepsilon - \|x_{i+k} - x_{j+k}\|_\infty)$, then the relation between I_l^μ and I_l is
 570 described by

$$\begin{aligned}
(i, j) \in I_l &\Leftrightarrow \theta_{-1} = \theta_l = 0 \quad \text{and} \quad \Theta(\varepsilon - \|\vec{x}_{i+k} - \vec{x}_{j+k}\|_\infty) = 1 \quad \text{for all } k = 0, \dots, l-1 \\
&\Leftrightarrow \theta_{-1} = \theta_l = 0 \quad \text{and} \quad \Theta(\varepsilon - \|\vec{x}_{i+k}^\mu - \vec{x}_{j+k}^\mu\|_\infty) = 1 \quad \text{for all } k = 0, \dots, l-\mu \\
&\Leftrightarrow \theta_{-1} = \theta_l = 0 \quad \text{and} \quad \sum_{k=0}^{l-\mu} \Theta(\varepsilon - \|\vec{x}_{i+k}^\mu - \vec{x}_{j+k}^\mu\|_\infty) = l - \mu + 1
\end{aligned} \tag{13}$$

$$\Leftrightarrow (i+k, j+k) \in I_l^\mu \quad \text{for all } k = 0, \dots, l-\mu. \tag{14}$$

571 Moreover, note that by construction $I_{l_1}^\mu \cap I_{l_2}^\mu = \emptyset$ for $l_1 \neq l_2$ and $\bigcup_{l \geq \mu} I_l^\mu =$
572 I^μ :

$$I_{l_1}^\mu \cap I_{l_2}^\mu = (I^\mu \cap J_{l_1}) \cap (I^\mu \cap J_{l_2}) \subset (J_{l_1} \cap J_{l_2}) = \emptyset \quad \text{for } l_1 \neq l_2, \tag{15}$$

$$\bigcup_{l \geq \mu} I_l^\mu = \bigcup_{l \geq \mu} I^\mu \cap J_l = I^\mu \cap \bigcup_{l \geq \mu} J_l = I^\mu. \tag{16}$$

573 Now we have collected all relations to begin the actual proof. Since

$$P(l) = |I_l| = \sum_{(i,j) \in I_l} 1 \stackrel{(13)}{=} \sum_{(i,j) \in I_l} \frac{\sum_{k=0}^{l-\mu} \Theta(\varepsilon - \|\vec{x}_{i+k}^\mu - \vec{x}_{j+k}^\mu\|_\infty)}{l - \mu + 1},$$

574 we get

$$(l - \mu + 1)P(l) = \sum_{(i,j) \in I_l} \sum_{k=0}^{l-\mu} \Theta(\varepsilon - \|\vec{x}_{i+k}^\mu - \vec{x}_{j+k}^\mu\|_\infty)$$

575 and therefore

$$\begin{aligned}
\sum_{l \geq \mu} (l - \mu + 1)P(l) &= \sum_{l \geq \mu} \sum_{(i,j) \in I_l} \sum_{k=0}^{l-\mu} \Theta(\varepsilon - \|\vec{x}_{i+k}^\mu - \vec{x}_{j+k}^\mu\|_\infty) \\
&\stackrel{(14)}{=} \sum_{l \geq \mu} \sum_{(i,j) \in I_l^\mu} \Theta(\varepsilon - \|\vec{x}_i^\mu - \vec{x}_j^\mu\|_\infty) \\
&\stackrel{(15)}{=} \sum_{(i,j) \in \bigcup_{l \geq \mu} I_l^\mu} \Theta(\varepsilon - \|\vec{x}_i^\mu - \vec{x}_j^\mu\|_\infty) \\
&\stackrel{(16)}{=} \sum_{(i,j) \in I^\mu} \Theta(\varepsilon - \|\vec{x}_i^\mu - \vec{x}_j^\mu\|_\infty) \\
&= \mathcal{PP}^{(\mu)}.
\end{aligned}$$

576 Rearranging this equation leads to

$$\sum_{l \geq \mu} lP(l) = \mathcal{P}\mathcal{P}^{(\mu)} + (\mu - 1) \sum_{l \geq \mu} P(l), \quad (17)$$

577 and it remains to show that

$$\mathcal{P}\mathcal{P}^{(\mu)} - \mathcal{P}\mathcal{P}^{(\mu+1)} = \sum_{l \geq \mu} P(l).$$

578 But this already follows by applying (17) for μ and $\mu + 1$:

$$\begin{aligned} \mathcal{P}\mathcal{P}^{(\mu)} - \mathcal{P}\mathcal{P}^{(\mu+1)} &= \sum_{l \geq \mu} lP(l) - (\mu - 1) \sum_{l \geq \mu} P(l) - \left(\sum_{l \geq \mu+1} lP(l) - \mu \sum_{l \geq \mu+1} P(l) \right) \\ &= \sum_{l \geq \mu} lP(l) - (\mu - 1) \sum_{l \geq \mu} P(l) - \left(\sum_{l \geq \mu} lP(l) - \mu P(\mu) - \mu \sum_{l \geq \mu} P(l) + \mu P(\mu) \right) \\ &= \sum_{l \geq \mu} P(l). \end{aligned}$$

579

□

580 **11. Appendix B - Example**

581 Assume that we want to compute the determinism of the sample trajectory
 582 $\vec{x} = (0.5, 0.8, 0.4, 0.6, 0.8, 0.4, 0.9)$, given a similarity threshold $\varepsilon = 0.1$. First
 583 we consider the recurrence plots

584
$$R_{i,j}^{(\nu)} := \Theta(\varepsilon - \|\vec{x}_i^\nu - \vec{x}_j^\nu\|_\infty), \quad \tilde{R}_{i,j}^{(\nu)} := \Theta(-\|\tilde{x}_i^\nu - \tilde{x}_j^\nu\|_\infty) \quad (18)$$

585 of the embedded (3) trajectory \vec{x}^ν and its discretization $\tilde{x}^\nu = \Phi_\delta(\vec{x}^\nu)$, where $\delta =$
 586 0.2 (see (8) and Sec. 5.2.1). The embedded trajectories and the corresponding
 587 recurrence plots are illustrated in Fig. 6 for several embedding dimensions $\nu =$
 588 $1, 2, 3$ in black, blue, and orange color, respectively. For example the recurrence
 589 plots for $\nu = 2$ comprise the recurrences marked by blue color, the black only
 590 highlighted entries are no recurrences for $\nu = 2$.

For $\nu = 1$ (write $\mathbf{R} = \mathbf{R}^{(1)}$) we observe that $R_{1,4} = 1$, but $\tilde{R}_{1,4} = 0$. That means the pair $(0.5, 0.6)$ is similar, i.e.,

$$|0.5 - 0.6| = 0.1 \leq \varepsilon,$$

but classified as dissimilar:

$$\Phi_\delta(0.5) = \left\lfloor \frac{0.5}{0.2} \right\rfloor = 2 \neq 3 = \left\lfloor \frac{0.6}{0.2} \right\rfloor = \Phi_\delta(0.6).$$

591 Due to symmetry the pairs $(0.5, 0.6)$ and $(0.6, 0.5)$ lead to $C(S, \neg S)$ -errors (see
 592 section 5.2). For all other pairs the classified and actual similarity statements
 593 coincide.

594 Recall that the determinism is the ratio between the number of points on
 595 diagonal lines and all points in the recurrence plot. For the non-embedded
 596 trajectories $\vec{x} = \vec{x}^1$ and $\tilde{x} = \tilde{x}^1$ we obtain by counting the structures in the
 597 recurrence plots:

598
$$DET^{(2)} = \frac{17}{21} \approx 0.81, \quad \tilde{DET}^{(2)} = \frac{15}{19} \approx 0.79. \quad (19)$$

599 Of course we have calculated the approximation inefficiently by employing
 600 the recurrence plot \mathbf{R} . Using Theorem 2 and Algorithm 1 we may compute
 601 $\tilde{DET}^{(2)}$ algorithmically:

602 Following Algorithm 1 we assign unique identifiers to the rows of \tilde{x}^ν . Note
 603 that in Fig. 7 the \vec{x}^ν are transposed, hence in this case we are interested in
 604 unique columns. The histograms of the identifiers (col_ID) are charged and
 605 due to Theorem 1 we calculate (compare with Fig. 7)

- 606 $\bullet \tilde{\mathcal{P}}\tilde{\mathcal{P}}^{(1)} = 3^2 + 3^2 + 1^2 = 19$
 607 $\bullet \tilde{\mathcal{P}}\tilde{\mathcal{P}}^{(2)} = 2^2 + 2^2 + 1^2 + 1^2 = 10$
 608 $\bullet \tilde{\mathcal{P}}\tilde{\mathcal{P}}^{(3)} = 1^2 + 1^2 + 1^2 + 1^2 + 1^2 = 5$

609 Finally, using Definition 1 (which is based on Theorem 2) we get the same result
 610 as before in Eq. (19):

611
$$DET^{(2)} = \frac{2 \cdot \tilde{\mathcal{P}}^{(2)} - (2-1) \cdot \tilde{\mathcal{P}}^{(3)}}{\tilde{\mathcal{P}}^{(1)}} = \frac{15}{19} \approx 0.79.$$

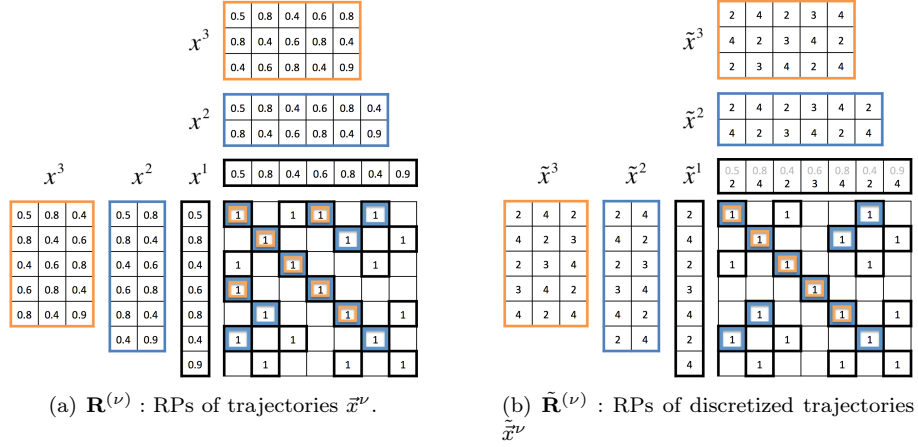


Figure 6: Recurrence Plots (RPs) of the recurrence matrices from Eq. (18) for $\nu = 1, 2, 3$, illustrated in black, blue, orange, respectively.

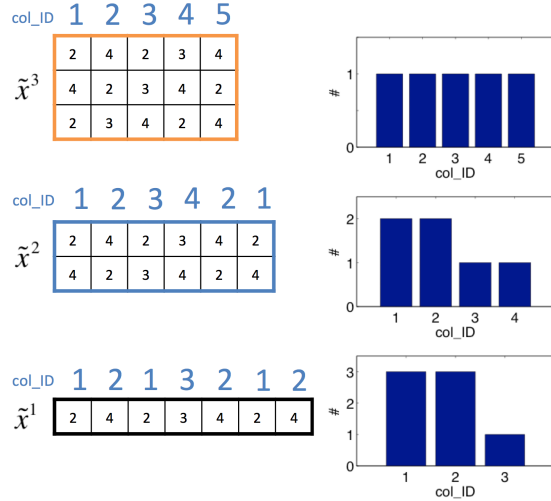


Figure 7: Histograms of trajectory embedding vectors.